

Variations to calcareous nannofossil CaCO_3 content during the middle Eocene C21r-H6 hyperthermal event (~ 47.4 Ma) in the Gorrondatxe section (Bay of Biscay, western Pyrenees)



Beñat Intxauspe-Zubiaurre^{a,*}, José-Abel Flores^b, Aitor Payros^c

^a Euskal Herriko Unibertsitatea Zientzia eta Teknologia Fakultate Estratigrafia eta Paleontologia Saila, Barrio Sarriena, s/n 48940 Leioa (Bizkaia), Spain

^b Departamento de Geología, Facultad de Ciencias Químicas, Universidad de Salamanca, Plaza de los Caídos s/n, 37003 Salamanca, Spain

^c Department of Stratigraphy and Paleontology, Faculty of Science and Technology, University of the Basque Country (UPV/EHU), P.O. Box 644, E-48080 Bilbao, Spain

ARTICLE INFO

Keywords:
Acidification
Lysocline
Coccolith
Carbonate mass
Image analysis
Eocene

ABSTRACT

The carbonate content of calcareous nannofossils is dependent on seawater composition. One of the factors that affect seawater chemistry and consequently the degree of calcification in coccolithophores is temperature, as seen in present day warming oceans. The depth at which carbonates are dissolved (Calcite Compensation depth, CCD) can rise due to an increase in HCO_3^- and decrease in pH, leading to a major dissolution on the seabed and burndown. Similar processes have also been deduced for Eocene hyperthermal events, such as the PETM and ETM2. This study reports changes in coccolith carbonate mass from a hemipelagic setting (Gorrondatxe, at 1500 m paleodepth) during the core of a minor Eocene hyperthermal event, namely the C21r-H6 event (47.44–47.32 Ma). Image analysis techniques were used to determine differences in the carbonate mass of selected calcareous nannofossil taxa, revealing species-specific patterns. The CaCO_3 mass of *Chiasmolithus solitus* decreased by 50% over the course of the C21r-H6 event, and many specimens also lost their crossed central bars, an additional indication of mass loss; *Reticulofenestra* sp. (3–5 μm) showed a similar trend, but the percentage of mass lost was lower; *Toweius pertusus*, interpreted as being reworked, mirrored the behaviour of *Chiasmolithus solitus*, suggesting that the CaCO_3 mass loss may have occurred on the seabed, rather than in the water column. In general, it can be concluded that the lysocline rose to 1500 m paleobathymetry in the Bay of Biscay during the C21r-H6 event. Formation of corrosive bottom water in the North Atlantic Ocean is regarded as being responsible for the rise in the lysocline.

1. Introduction

Eocene hyperthermal events were geologically short-lived (10–200 kyr-long) global warming episodes caused by the injection of greenhouse gases into the atmosphere (Cramer et al., 2003; Dickens, 2003; Lourens et al., 2005; Niclou et al., 2007; Röhl et al., 2005; Thomas and Zachos, 2000; Westerhold et al., 2007; Zachos et al., 2001). The geochemical records obtained from the hyperthermal event sediments suggest that significant environmental changes affected both the oceans and the biosphere (Denman et al., 2007; Dunkley Jones et al., 2013; Kirtland Turner et al., 2014; Sluijs et al., 2007a, 2007b; Zeebe, 2013). For example, geochemical studies have shown that an increase in pCO_2 contributed to ocean acidification during some of the hyperthermal events (Dickens et al., 1997; Leon-Rodriguez and Dickens, 2010; Penman et al., 2014; Zachos et al., 2005). Accordingly, today's increase in the concentration of atmospheric CO_2 concentration is

reportedly leading to an increase in seawater pCO_2 (Archer, 1999; Caldeira and Wickett, 2005; Höönsch et al., 2012; Kump et al., 2009; Sarmiento et al., 1992; Weiss, 1974), which has raised the calcite compensation depth (CCD) level, the depth at which carbonate is absent (Maier-Reimer and Hasselmann, 1987; Rudimann, 2001; Orr et al., 2005). The lysocline, the depth at which carbonate dissolution increases remarkably, has risen accordingly, affecting some calcareous organisms that inhabit seabed environments (Archer, 1999; Raffi et al., 2005; Rudimann, 2001). In addition, ocean acidification changes the physiology of many organisms and threatens the survival of the entire ecological community.

Dissolution on the seabed also occurred during some of the Eocene hyperthermal events. For example, during the Paleocene-Eocene Thermal Maximum (PETM) and the Eocene Thermal Maximum 2 (ETM2), the most intense and best known of the Eocene hyperthermal events, deep-sea sediments found to be lacking in carbonate were

* Corresponding author.

E-mail address: benat.intxauspe@ehu.eus (B. Intxauspe-Zubiaurre).

relatively common (Kelly et al., 2012; Lunt et al., 2012; Milliman, 1999; Pälike et al., 2012; Zeebe and Zachos, 2007). This demonstrates that deep-sea areas in which carbonate sediments accumulated under normal conditions were subject to CaCO_3 dissolution during the hyperthermal events (i.e. ODP Leg 198 at Shatsky Rise, Colosimo et al., 2006). The good connection between oceans permitted that carbonate dissolution was widespread, but occurred at different depths in different locations (Pälike et al., 2012; Sluijs et al., 2007b; Zachos et al., 2005).

Geochemical proxies (e.g. $\delta^{18}\text{O}$, $\delta^{13}\text{C}$, CaCO_3 content) have shown that the rise in temperature during the abovementioned Eocene hyperthermal events (e.g., 5–8 °C during the PETM; 3–5 °C during ETM2) was more intense than today's global warming episode (Forster et al., 2007; Galeotti et al., 2010; Keeling and Whorf, 2004; Lei et al., 2016; Lourens et al., 2005; Westerhold et al., 2007). Consequently, the study of less intense hyperthermal events is necessary to understand the potential response of the environment to current global warming. To this end, the present study characterizes one of the less intense Eocene hyperthermal events, specifically the core of the so-called C21r-H6 event (47.44–47.32 Ma, early Lutetian, middle Eocene). This event was first described by Sexton et al. (2011) as a hyperthermal event produced by a perturbation in the global carbon-cycle. In the equatorial western Atlantic Ocean (ODP Site 1258) this event is characterized by a 0.7‰ decrease in benthic foraminiferal $\delta^{13}\text{C}$ and a decrease of 0.4‰ in benthic foraminiferal $\delta^{18}\text{O}$ (Sexton et al., 2011), suggesting a 2 °C warming in bottom waters, whereas in the South Atlantic (ODP Sites 1262–1267), Southern Ocean (ODP Site 690) and the Pacific (ODP Sites 1215–1222) it is characterized by carbonate dissolution at 2000–3000 m paleodepth, pointing to a global increase in deep ocean acidity and a rise in the lysocline (Bains et al., 1999; Rea and Lyle, 2005; Zachos et al., 2005). Payros et al. (2012) identified and described the C21r-H6 event at the Gorrondatxe cliff section (south-eastern coast of the Bay of Biscay, western Pyrenees; Fig. 1). Subsequently, Intxauspe-Zubiaurre et al. (2017) analyzed the variations of calcareous nannofossil assemblages and their relationship with paleoenvironmental changes across the C21r-H6 event at Gorrondatxe.

This study aims to identify changes in seawater chemistry by analyzing coccolith CaCO_3 content. Calcareous nannofossils, particularly coccolithophores, are the main primary organic CaCO_3 producers of calcium carbonate in the oceans (Baumann et al., 2005; Westbroek et al., 1994; Ziveri et al., 1999). Their production (calcification) and dissolution are directly affected by changes in CaCO_3 equilibrium conditions in seawater (Gibbs et al., 2010; Jiang and Wise, 2006; Meyer and Riebesell, 2015; Mutterlose et al., 2007; Raffi and de Bernardi, 2008; Ridgwell and Schmidt, 2010; Riebesell, 2004; Thierstein and Young, 2004). On the one hand, HCO_3^- availability and pCO_2 in the seawater affect coccolith calcite production (Riebesell, 2004; Riebesell et al., 2000; Rost and Riebesell, 2004; Stoll et al., 2007; Monteiro et al., 2016). On the other hand, corrosive waters with low pH cause coccolith malformations and CaCO_3 loss after death (Agnini et al., 2016; Beaufort et al., 2011; Bralower and Self-Trail, 2016; Hassenkam et al., 2011). Thus, calcareous nannofossils constitute a useful tool by which changes in seawater CaCO_3 chemistry can be determined. The present study aims to approach changes in both coccolith CaCO_3 production and dissolution.

2. Regional setting

The studied succession is exposed on the cliff of the Gorrondatxe beach (43° 23'N 3° 01'W; Fig. 1), which hosts the Global Stratotype Section and Point of the base of the Lutetian Stage (Molina et al., 2011). This section is part of a 2300-m-thick deep-marine sedimentary succession accumulated on a rapidly subsiding basin during early-middle Eocene (Payros et al., 2006). Located at the bottom of a 1500 m deep gulf that opened into the Atlantic Ocean at 35°N paleolatitude (Smith, 1996), the area was part of the North Iberian continental margin.

The lower Lutetian succession in Gorrondatxe is composed of alternating pelagic limestones and marls interspersed with thin-bedded turbidites, which form recurrent tripartite sequences, generally 10–40 cm thick, consisting of a basal thin-bedded sandy turbidite (with divisions Ta to Td of the Bouma sequence) capped with a layer of grey clay (division Te of the Bouma sequence) and a layer of whitish pelagic mudstone (Payros et al., 2007, 2009; Payros and Martínez-Bráceras, 2014). The sediments accumulated during the core of the C21r-H6 event (118–133 m of the succession; Figs. 1 and 2) are characterized by a distinctively low carbonate content and increased abundance of turbidites and kaolinite. This interval is also typified by an abrupt decline (1‰) in benthic foraminiferal $\delta^{13}\text{C}$ (Fig. 2) and an increase in foraminiferal fragmentation index (Payros et al., 2012). Calcareous nannofossils show a decrease in the abundance of oligotrophic taxa and increased abundance of reworked and epicontinental specimens, strongly suggesting increased continental input (Intxauspe-Zubiaurre et al., 2017).

3. Biostratigraphy and biochronology

According to previous works (Bernaola et al., 2006; Intxauspe-Zubiaurre et al., 2017), the presence of *Nannotetraena cristata* and *Blackites inflatus* and the absence of *Nannotetraena alata* and *Blackites gladius* place the studied succession within the biostratigraphic zones NP14 and CP12b (Martini, 1971; Okada and Bukry, 1980), and more specifically within the *Helicosphaera lophota* Subzone (Bown, 1998) or Zone CNE 8 – *Nannotetraena cristata* Base Zone (Agnini et al., 2014). Bernaola et al. (2006) also showed that the lowermost 142 m of the Gorrondatxe section are characterized by reverse magnetic polarity, whereas the uppermost 58 m show normal magnetic polarity. Based on biostratigraphic data, these intervals were placed in chrons C21r and C21n, respectively. In addition, Payros et al. (2007, 2009) identified precession-related 21 kyr-long limestone–marl couplets and eccentricity-related 100 kyr-long bundles. Using a cyclostratigraphic approach, Payros et al. (2012) calculated that the onset of the C21r-H6 event occurred at 47.44 Ma, uppermost part of Chron C21r (Gradstein et al., 2012), extending along 120 kyr.

4. Material and methods

One hundred and twenty-eight samples were collected from an 82 m thick section, between 98 and 180 m (Fig. 2), which document the pre-C21r-H6 interval (98–118 m), the sediments of the core of the C21r-H6 event (118–133 m), and the lowermost sediments of the post-event interval (133–182 m). However, sampling resolution varied along the section. In most of the pre-event interval (from 98 to 114 m) samples were collected every 80 cm. The sample spacing was reduced to 30 cm in the uppermost 4 m of the pre-event sediments and throughout the C21r-H6 event interval (114–133 m). Sample spacing increases again to 80 cm in the lowermost 29 m of the post-event interval (133–162 m). In the rest of the studied sequence, spacing progressively increased from 1.4 m to 2 m. According to the 10.8 cm/kyr average sedimentation rate calculated by Payros et al. (2015) for the studied interval, the time lapse between samples was 2.8 kyr in the C21r-H6 core sediments, 7.4 kyr in the underlying and overlying intervals, and progressively increased from 13 to 18 kyr in the uppermost part of the succession. Given that pelagic mudstones were too hard for the extraction of microfossils, all samples were collected at the transitions from turbiditic grey marls to their overlying whitish pelagic mudstones, where primary mixing and the addition of allochthonous specimens by turbidity currents are assumed to be minimal.

The samples were dried in an oven and subsequently 4 mg were extracted using a surgery knife and distributed homogeneously on a coverslip, following the decantation method proposed by Flores and Sierro (1997). Coverslips were then glued to a smear slide using Canada balsam.

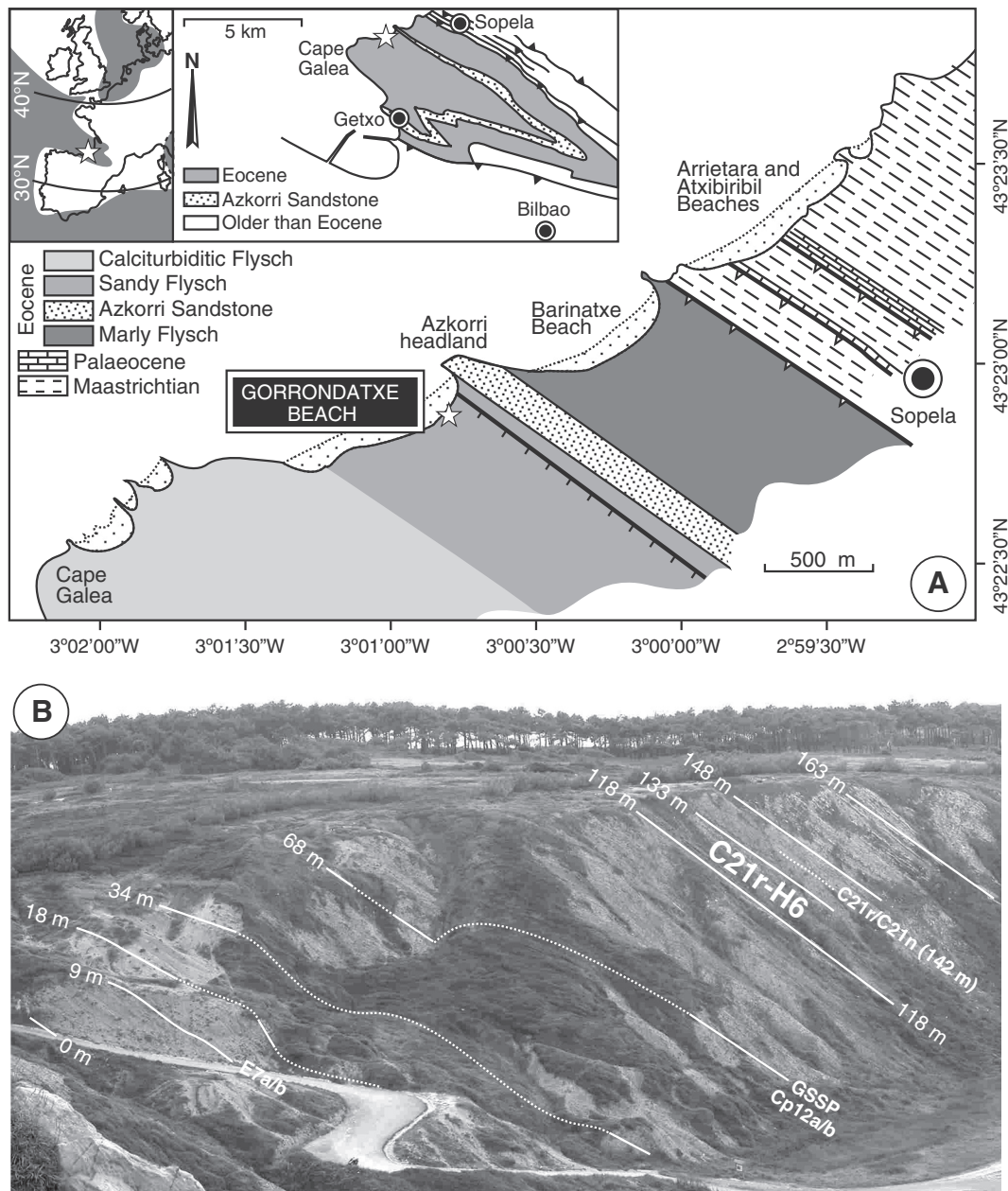


Fig. 1. (A) Simplified Eocene paleogeographic and geological maps of the Gorrondatxe area, showing (paleo)location of the studied section (star). (B) General view of the Gorrondatxe section, showing reference levels and the location of the core of the C21r-H6 event. (Figure modified from Payros et al., 2012).

The coccolith carbonate mass analysis was carried out using the image analysis technique proposed by Fuertes et al. (2014). This technique measures the quantity of light transmitted by the coccolith, which directly depends on coccolith thickness (Beaufort et al., 2014). The measurement consisted of the following steps: Firstly, coccolith images were captured, for which a Nikon Eclipse LV100POL microscope and the program NISElements were used. In order to avoid interference figures of the coccoliths in greyscale, the images were captured under circularly polarized light with crossed nicols (Fuertes et al., 2014). Fig. 3 shows the differences of the calcareous nannofossil images under linearly and circularly polarized light. Fifty images of every taxon were captured on each sample at 1000 \times magnification.

Secondly, the volume of each coccolith was estimated from the captured image using C-Calcita software (Fuertes et al., 2014). To this end, greyscale shades of each image were classified into 256 levels, in which the highest value corresponded to white and the lowest to black.

The highest values correlated with the thickest calcite, whereas lower values represented thinner calcite. The sum of the grey level of each pixel within a given coccolith led to the total volume and mass of the specimen (Fig. 4). Additionally, the number of pixels that made up the coccolith was regarded as a proxy value for the surface area of the specimen, which allowed calculation of its mass/area index. Finally, the mean mass/area index of the 50 images captured of each taxon was calculated for each smear slide. After a pilot survey of several taxa, the work focused on three taxa (Fig. 5), of which 6400 images were captured for each and analyzed following the method described above. This automated technique provides direct values of the CaCO₃ mass content of selected specimens, saving considerable time compared to non-automated measurement techniques.

Two of the selected taxa, namely *Reticulofenestra* sp. (3–5 µm) and *Chiasmolithus solitus*, were autochthonous, and can therefore record changes in CaCO₃ chemistry that occurred both during the life span of

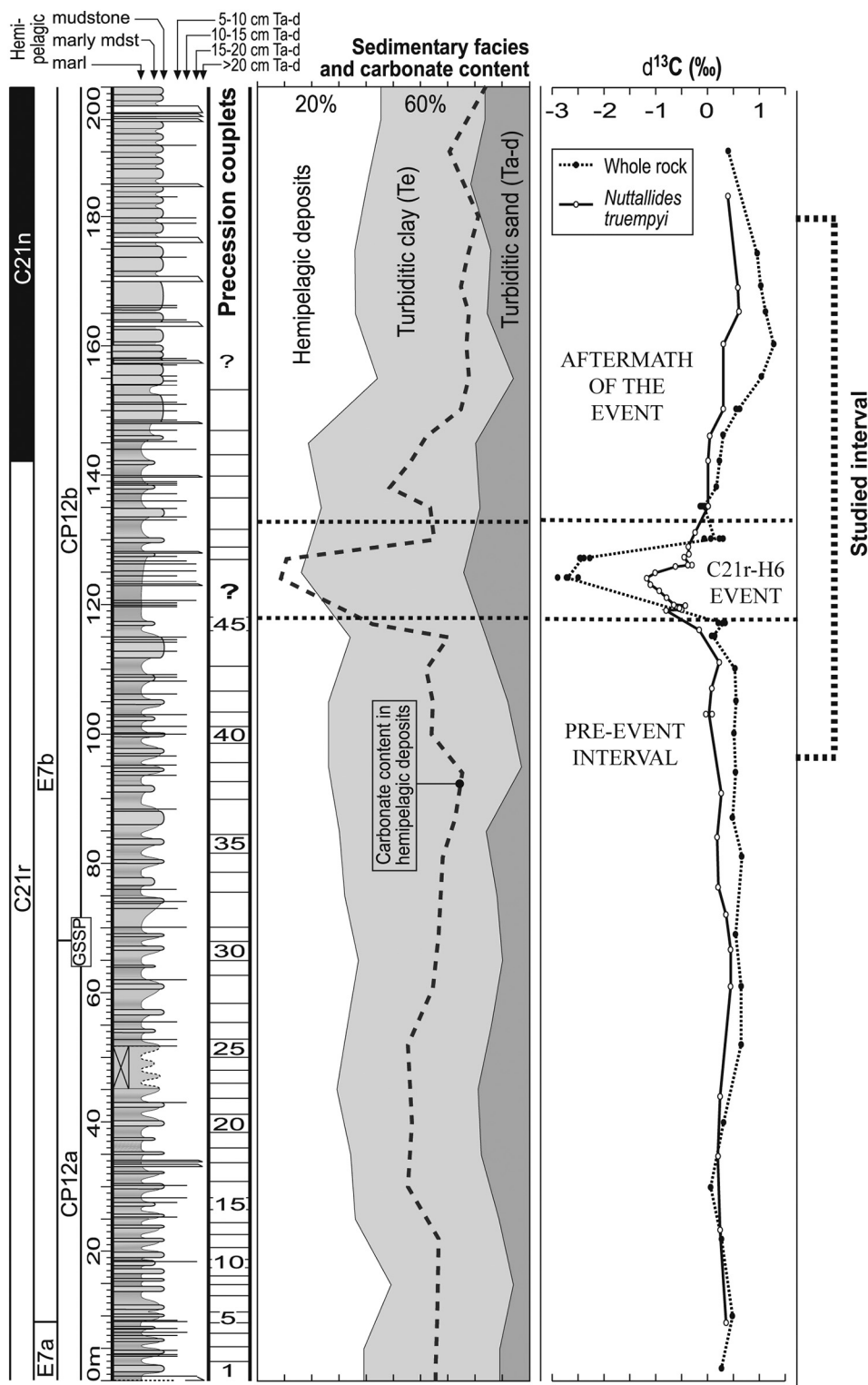


Fig. 2. Previous data from the Gorrondatxe section (compiled from Payros et al., 2012), showing the lithological log, chronostratigraphy, precession-driven mudstone-marl couplets, variations in the percentage of turbiditic and hemipelagic sediments, and their carbonate content. Stable isotope ($\delta^{13}\text{C}$) results were obtained from both hemipelagic mudstones (whole rock) and from the benthic foraminifer *Nuttallides truempyi*. The succession studied herein extends from 98 to 180 m.

the specimens and after their death. The third taxon is *Toweius pertusus*, interpreted here as reworked, which can only record postmortem processes. This species was selected on the basis of its dissolution-prone nature (Adelseck et al., 1973; Jiang and Wise, 2006; Raffi et al., 2009; Stoll et al., 2007; Tremolada and Bralower, 2004).

The mass/area index results of the abovementioned taxa were plotted on graphs in order to represent the evolution of the mean mass/area index across the successive intervals of the succession (Fig. 6). In order to have an additional dissolution proxy linked to coccoliths, the

occurrence of crossed central bars in *Chiasmolithus solitus* was also analyzed (Fig. 5), as their absence is regarded as an indication of dissolution (Adelseck et al., 1973; Gibbs et al., 2004; Perch-Nielsen, 1985; Raffi and de Bernardi, 2008). Therefore, the percentage of *Chiasmolithus solitus* without crossed central bars per smear slide was calculated (Fig. 6).

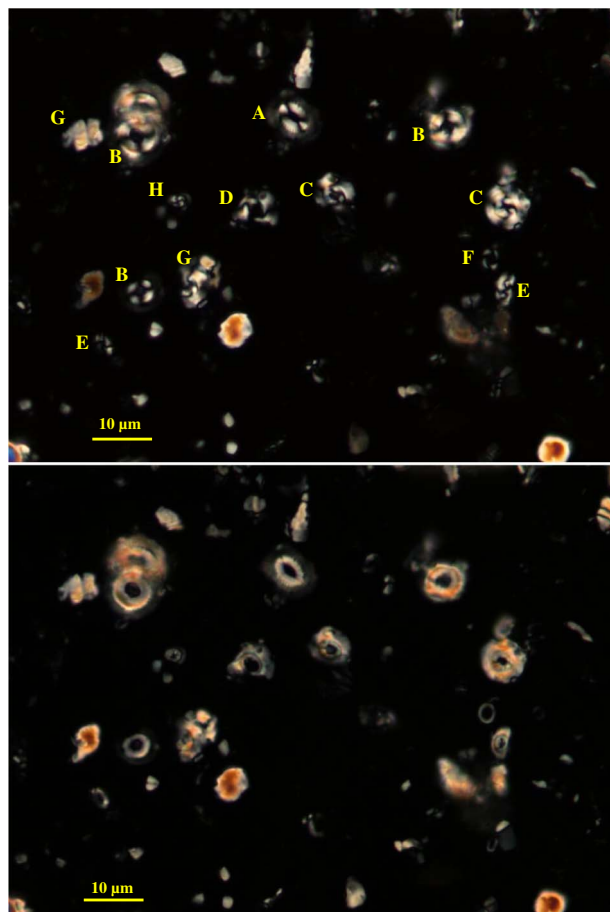


Fig. 3. Microphotographs of sample collected at 107.5 m under linearly polarized light (above) and circularly polarized light (below). Note the difference between the interference figure and real image in the following taxa: (A) *Coccilithus pelagicus*, (B) *Coccilithus formosus*, (C) *Reticulofenestra dictyoda* with restricted central area, (D) *Reticulofenestra dictyoda* with open central area, (E) *Reticulofenestra minuta*, (F) *Umbilicosphaera bramlettei*, (G) *Zygrhablithus bijugatus*, and (H) *Toweius pertusus*. Scale bar 10 μm .

5. Results

Calcareous nannofossil preservation was moderate, but no overgrowth was observed, allowing a reliable identification of the taxa. The mean mass/area index of *Chiasmolithus solitus* decreased significantly at the C21r-H6 event sediments (Fig. 6). The average mass/area index in the pre-event interval was 1.26 $\text{pg}/\mu\text{m}^2$, reaching a maximum value of 1.79 $\text{pg}/\mu\text{m}^2$ at 102 m and showing two smaller but consecutive peaks of 1.37 and 1.54 $\text{pg}/\mu\text{m}^2$ at 113 and 116 m, respectively. The mean mass/area index value decreased to 0.88 $\text{pg}/\mu\text{m}^2$ during the C21r-H6 event, with a minimum value of 0.51 $\text{pg}/\mu\text{m}^2$ at 122 m. Interestingly, this minimum value is less than a third of the maximum pre-event value. The mean mass/area index rose to 0.97 $\text{pg}/\mu\text{m}^2$ in the post-event interval. The evolution of the average mass/area index of *Chiasmolithus solitus* along the succession was in line with the results obtained in the analysis of its crossed central bars. Thus, only 3% of the specimens lack their crossed central bars in the pre-event interval, but 12% do not have their cross structure in the C21r-H6 interval, peaking at 35% at the core of the event (121 m to 126 m). Subsequently, the percentage of *Chiasmolithus solitus* with no crossed central bars decreased to 7.5% in the post-event interval.

The overall trend shown by the evolution of the mass/area index of *Reticulofenestra* sp. (3–5 μm) is to some extent similar to that of *Chiasmolithus solitus*. For example, peak values are reached at 102, 113 and 116 m of the pre-event interval, whereas the lowermost part of the

C21r-H6 interval shows lower values. However, absolute average values do not show significant variations throughout the succession, the mean mass/area index being 0.95 $\text{pg}/\mu\text{m}^2$ in the pre-event interval, 0.9 $\text{pg}/\mu\text{m}^2$ in the C21r-H6 interval, and 0.89 $\text{pg}/\mu\text{m}^2$ in the post-event interval. In addition, the minimum value of the mass/area index of *Reticulofenestra* sp. (3–5 μm) within the C21r-H6 interval (0.58 $\text{pg}/\mu\text{m}^2$ at 125 m) is not as low as that of *Chiasmolithus solitus*.

The overall trend is also mirrored by reworked *Toweius pertusus*. Its mean mass/area index was 1.11 $\text{pg}/\mu\text{m}^2$ in the pre-event interval, peaking at 1.36 and 1.22 $\text{pg}/\mu\text{m}^2$ at 113 and 116 m, respectively. The value decreased to 0.99 $\text{pg}/\mu\text{m}^2$ in the C21r-H6 interval, reaching a minimum value of 0.80 $\text{pg}/\mu\text{m}^2$ at 121 m. Finally, the mean mass/area index of *Toweius pertusus* rose back to 1.12 $\text{pg}/\mu\text{m}^2$ in the post-event interval.

To sum up, the three taxa analyzed herein showed similar mass/area index trends throughout the section. Their mean mass/area indices peaked slightly before the C21r-H6 event, but decreased significantly during the event, increasing again in the post-event interval.

6. Discussion

6.1. Dissolution vs. calcification

The estimates of coccolith mass obtained in this study are highly significant, as their CaCO_3 content decreased during the C21r-H6 event. The loss of the crossed central bars in *Chiasmolithus solitus* at the C21r-H6 interval, along with the similar mass/area index trends in *Chiasmolithus solitus*, *Reticulofenestra* sp. and *Toweius pertusus*, suggest that the changes in CaCO_3 coccolith content in Gorrondatxe were related to dissolution.

The differences in mass loss between taxa are probably a consequence of their specific resistance to dissolution. *Chiasmolithus solitus* specimens lost up to two thirds of their original mass during the C21r-H6 event and a high percentage of the specimens completely lost their crossed central bars. Conversely, *Reticulofenestra* sp. does not show a significant decrease in mass/area index during the C21r-H6 event. We conclude that *Chiasmolithus solitus* is very susceptible to dissolution, while *Reticulofenestra* sp. is less affected. The decrease in the mass/area index in *Toweius pertusus* occurs parallel to that of *Chiasmolithus solitus*. Therefore, although dissolution of *Toweius pertusus* could have occurred before reworking, the similarity of the two proxies suggests that both taxa were affected by the same process during the C21r-H6 event. *Toweius pertusus* should also be classified as susceptible to dissolution, as suggested by many authors (Agnini et al., 2015; Gibbs et al., 2004; Perch-Nielsen, 1985; Raffi and de Bernardi, 2008).

Other processes could have influenced the variations in carbonate content of the coccoliths. Firstly, changes in seawater chemistry, possibly linked to the dissolution shown by the data, could have made coccolithophores produce either more or less calcite (Beaufort et al., 2014; Stoll et al., 2007; Thierstein and Young, 2004). Unfortunately, it is not yet well known whether coccolith calcification increases (Iglesias-Rodriguez et al., 2008; Langer et al., 2006; Rivero-Calle et al., 2015) or decreases (Beaufort et al., 2011; Bolton and Stoll, 2013; O'Dea et al., 2014; Raven and Crawford, 2012) in high pCO_2 conditions. Moreover, changes in the mass/area index could also be a result of diagenetic alteration. Our results only show the final carbonate content of coccoliths and cannot elucidate whether the observed stratigraphic trends are the result of life-cycle variations or taphonomic and diagenetic processes. In any case, post-mortem dissolution can be readily considered on the basis of the loss of the central cross in *Chiasmolithus solitus*.

6.2. Causes of dissolution

The precise location where the dissolution of calcareous nannofossils took place (water column, seabed, or both) cannot be readily determined. However, indirect evidence suggests that some dissolution

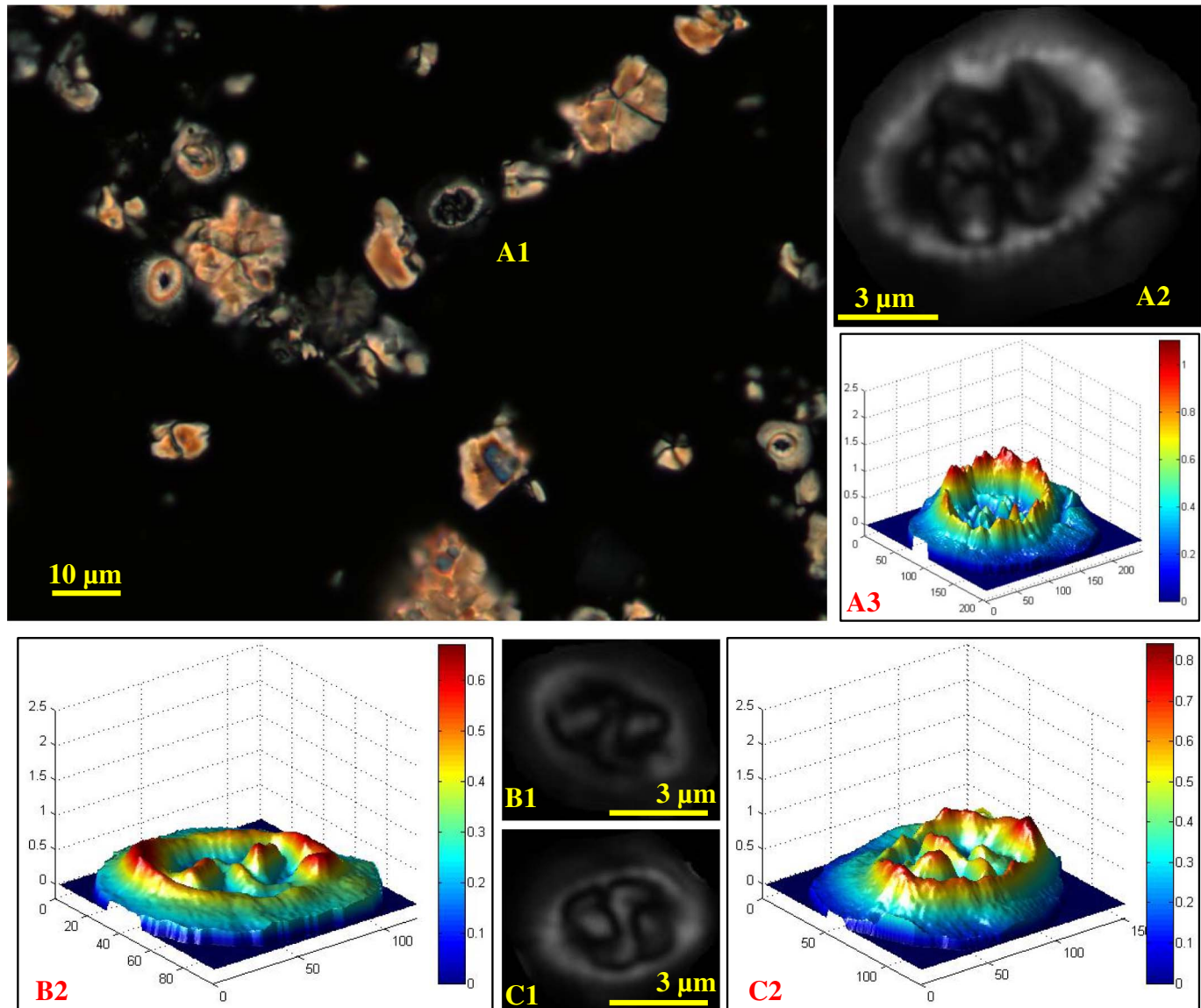


Fig. 4. Example of how coccolith volume and mass were estimated (coccoliths of *Chiasmolithus solitus* in sample collected at 107.5 m). (A1) Capture of a field of view under circularly polarized light. (A2) Image of *Chiasmolithus solitus* cut using C-Calcita software (Fuertes et al., 2014); note the differences in the greyness of each pixel. (A3) 3D reconstruction obtained from the image in A2. Other images of *Chiasmolithus solitus* are also shown (B1, B2) along with their respective 3D reconstructions (C1, C2). The thickness of the pixels is given in both the vertical scale bar (μm) and the colour scale (μm). The volume of the coccolith is obtained from the sum of the thickness of all pixels, whereas the mass is obtained by multiplying the volume with CaCO_3 density. The area of the coccolith corresponds to the surface of all the pixels with thickness $> 0 \mu\text{m}$ (measured in μm with the horizontal scale bar).

occurred on the seabed. Firstly, this scenario best explains the similar dissolution patterns observed in both autochthonous and reworked taxa; secondly, Payros et al. (2012) reported a distinct deterioration in calcareous foraminifera preservation within the C21r-H6 sediments, along with a significant increase in organic cemented agglutinated benthic foraminifera; finally, seabed carbonate dissolution was a common phenomenon during other Eocene hyperthermal events (Bralower et al., 2014; Dedert et al., 2014; Kennett and Stott, 1991; Stap et al., 2009).

Additional indirect evidence was derived from the comparison of the Gorrondatxe section with other areas. Sexton et al. (2011) reported increased carbonate dissolution at 2000–3000 m paleodepth in the South Atlantic and Pacific oceans during the C21r-H6 event (ODP Sites 1258 and 1210, respectively). Payros et al. (2012) added that a coeval carbonate-barren interval also occurred in the western North Atlantic Ocean (ODP Site 647, Labrador Sea, at present day 3800 m water depth; Firth et al., 2012). These characteristics point to a global increase in deep ocean acidity and a rise in the lysocline, which in all likelihood

reached the Gorrondatxe seabed at 1500 m water depth. In that case, dissolution should also be recorded in DSDP Site 401, located in the Bay of Biscay at 1800–2000 m paleodepth (Montadert and Roberts, 1979). Unfortunately, no carbonate-content data was given for the C21 Chron interval. Interestingly, however, carbonate content decreased from 80 to 30 wt% during the PETM (Bornemann et al., 2014) and from 80 to 40 wt% during the ETM2 (d'Haenens et al., 2014). These losses in CaCO_3 suggest that the lysocline rose, not completely removing carbonate from the seabed but nonetheless producing relevant dissolution.

Carbonate dissolution on the Gorrondatxe continental margin could also have increased due to local processes, such as corrosion by pore waters acidified during organic matter decay (Agnini et al., 2007, 2009; Bralower, 2002; Gibbs et al., 2006; Khalil and Al Sawy, 2014; Payros et al., 2015). In fact, increased continental runoff and weathering, combined with increased terrestrial input to the sea, including refractory organic matter and plant detritus, occurred during the C21r-H6 event in the Gorrondatxe area (Payros et al., 2012; Intxauspe-Zubiaurre et al., 2017). Similar processes were also reported during other

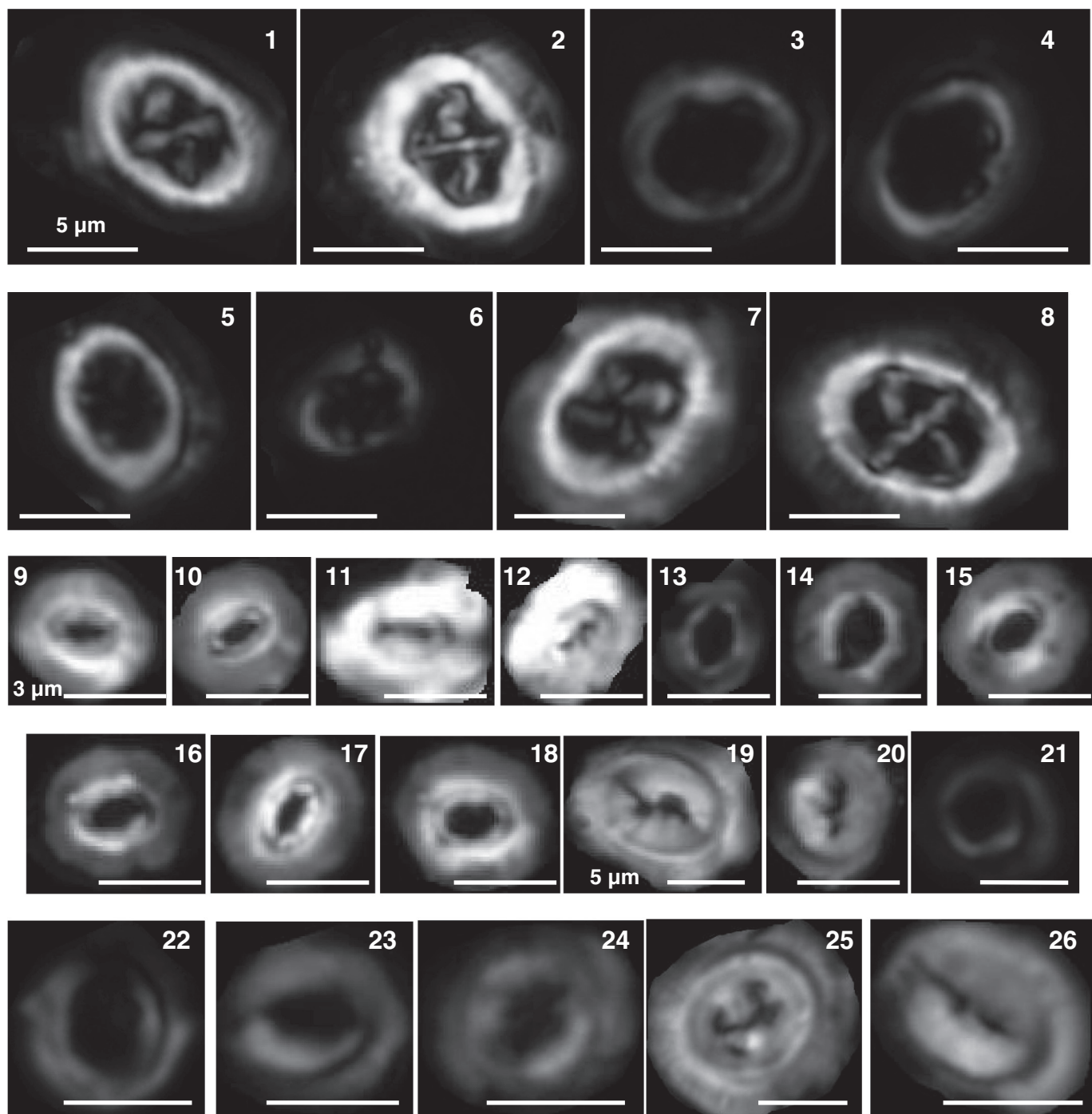


Fig. 5. Images of the analyzed taxa under circularly polarized light and cut using C-Calcita software (Fuertes et al., 2014). Note different levels of mass loss at the C21r-H6 Interval. (1–8) *Chiasmolithus solitus*. (1) Sample from the pre-event interval, 100.5 m. (2) Pre-event sample, 107.5 m. (3) Sample from the C21r-H6 interval, 122.7 m. (4) Sample from the C21r-H6 interval, 125.3 m. (5) Sample from the lower post-event interval, 135.5 m. (6) Lower post-event sample, 143.25 m. (7) Sample from the upper post-event interval, 156.7 m. (8) Upper post-event sample, 163.5 m. (9–18) *Reticulofenestra* spp. (3–5 μm). (9) Pre-event sample, 103.75 m. (10) Pre-event sample, 107.5 m. (11) Pre-event sample, 113 m. (12) Pre-event sample, 116 m. (13) Sample from the C21r-H6 interval, 122.1 m. (14) Sample from the C21r-H6 interval, 122.5 m. (15) Sample from the lower post-event interval, 139.5 m. (16) Lower post-event sample, 143.25 m. (17) Sample from the upper post-event interval, 156.7 m. (18) Upper post-event sample, 163.5 m. (19–26) *Toweius pertusus*. (19) Pre-event sample, 113 m. (20) Pre-event sample, 106.25 m. (21) Sample from the C21r-H6 interval, 121.6 m. (22) Sample from the C21r-H6 interval, 123.9 m. (23) Lower post-event sample, 140.75 m. (24) Lower post-event sample, 142.75 m. (25) Upper post-event sample, 155.75 m. (26) Upper post-event sample, 173 m. Scale bar 5 μm for *Chiasmolithus solitus*, 3 μm for *Reticulofenestra* spp., 5 μm for *Toweius pertusus*.

hyperthermal events (Giusberti et al., 2007; Kelly et al., 2005; Pujalte et al., 2016; Ravizza et al., 2001; Schmitz and Pujalte, 2003; Zachos et al., 2010).

Regardless of local factors, deep-sea carbonate dissolution during the C21r-H6 event can be considered as a global paleoceanographic process. During other early-middle Eocene hyperthermal events, deep-

sea dissolution was linked to shifts in the source areas of bottom waters. Paleoceanographic reconstructions have shown that during early-middle Eocene times deep-water formation generally occurred in the South Atlantic Ocean, from which the rest of the deep oceans were fed (Bice and Marotzke, 2000; Pak and Miller, 1992; Thomas et al., 2003). However, during the PETM and ETM2 hyperthermal events, significant

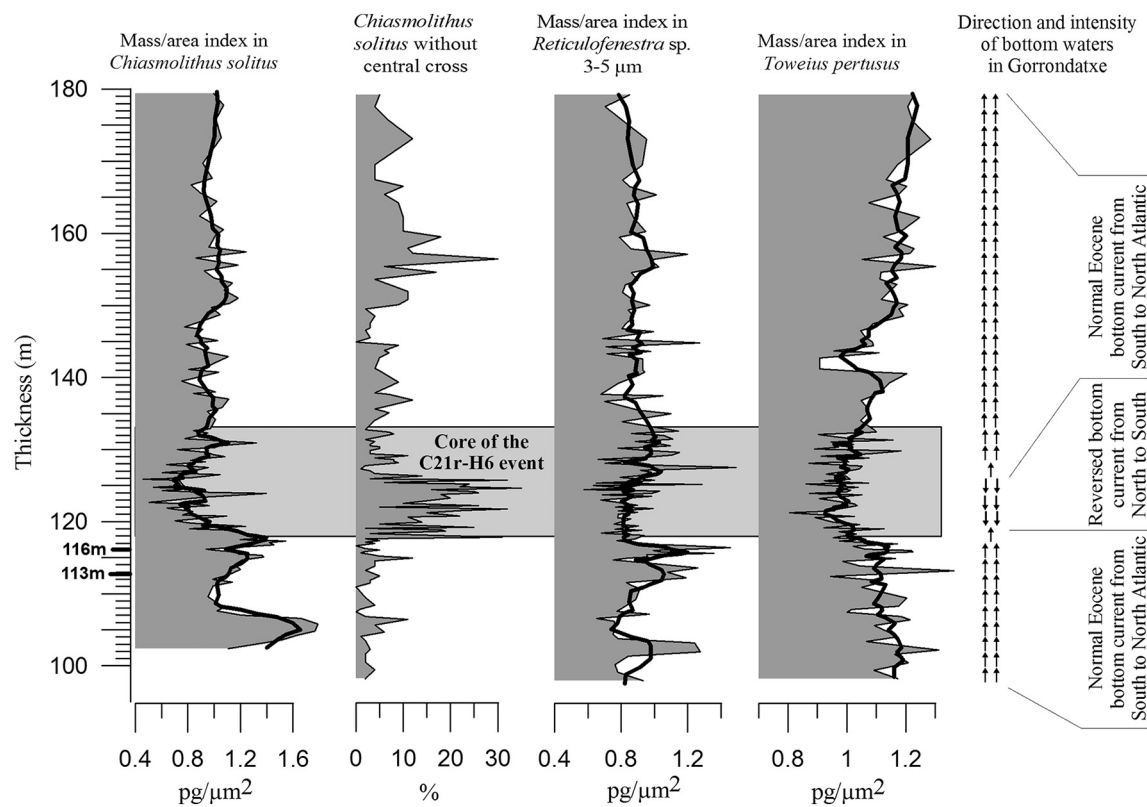


Fig. 6. Stratigraphic distribution of the mass/area index of the analyzed taxa. The thick black curves show 5-point running mean values and illustrate general trends. Note that scale-bars are different for each case. The second column shows the percentage of *Chiasmolithus solitus* specimens without crossed central bars. Arrows on the right indicate the direction of deep-sea bottom currents in the Gorrondatxe area: ↑↑ Bottom current from South to North, most common in Eocene times; ↑ Weakened South to North bottom current; ↓↓ Reversed bottom current from North to South during the C21r-H6 event.

shifts in oceanic currents occurred. Particularly, downwelling and deep-water formation in the South Atlantic Ocean weakened or even halted due to a rise of 6–7 °C in sea-surface temperature (Cope and Winguth, 2011; Zachos et al., 2008). Simultaneously, downwelling and deep-water formation started in the NW Atlantic ocean, where Tethyan and Arctic waters mixed (Alexander et al., 2015; Bice and Marotzke, 2002; d'Haenens et al., 2014; Jennions et al., 2015; Nunes and Norris, 2006; Sluijs et al., 2009; Tripati and Elderfield, 2005). These bottom water masses were characterized by high pCO₂, therefore having relatively low pH and being comparatively corrosive (Bralower et al., 2014; Kennett and Stott, 1991; Lunt et al., 2010; Schaller, 2015; Thomas and Shackleton, 1996). Several studies have shown that the formation of these northern Atlantic bottom waters raised the lysocline from approximately 2500 to < 2000 m water-depth during some of the Eocene hyperthermal events (e.g. Colosimo et al., 2006; d'Haenens et al., 2014; Ridgwell, 2007; Zachos et al., 2005; Zeebe et al., 2009).

Unfortunately, a detailed paleoceanographic reconstruction is not available for the period in which the C21r-H6 event occurred. Interestingly, however, coeval sediments from ODP Site 647, drilled on the flank of Gloria Drift in the southern Labrador Sea (NW Atlantic Ocean) are conspicuously carbonate barren, whereas both the underlying and overlying sediments do contain abundant carbonate components (Firth et al., 2012; Srivastava et al., 1987). Similar drift sediments have been reported from the nearby Newfoundland area (Norris et al., 2012) and from the Faroe-Shetland area in the NE Atlantic Ocean (Hohbein et al., 2012), all of which were demonstrated to have been active since the early-middle Eocene transition. These drift sediments were formed by pulses of strong bottom-flowing currents produced in the Norwegian-Greenland Sea, which spilled over the Greenland-Scotland Ridge. In addition, during the PETM global oceanic stratification produced by warming of the Southern Ocean surface waters resulted in weakened downwelling in the area. Simultaneously, salinity of surface

waters increased in the Atlantic and Tethys oceans. Several authors have suggested that these high-density saline warm waters, characterized by high pCO₂, sank in the NW Atlantic Ocean and contributed to the global oceanic circulation (Cope and Winguth, 2011; Nunes and Norris, 2006; Pak and Miller, 1992; Roberts et al., 2009). It is therefore very likely that high pCO₂, low-pH and corrosive deep-water masses also formed in the NW Atlantic Ocean during the C21r-H6 event. The circulation and spreading of these waters raised the CCD and lysocline globally, causing deep-sea carbonate dissolution worldwide.

7. Conclusions

Calcareous nannofossils from Gorrondatxe showed significant changes in mass/area index during the C21r-H6 event. All analyzed taxa showed similar trends throughout the succession, which included high pre-event mass/area index values (e.g., 113 and 116 m) and significant decreases within the C21r-H6 event. The mean mass/area index significantly decreased in *Chiasmolithus solitus* and up to 35% of the specimens lost their crossed central bars, which shows its susceptibility to dissolution. *Reticulofenestra* sp. (3–5 μm) shows a considerably smaller decrease in the mean mass/area index, suggesting a more dissolution-resistant nature. The mass/area index trend in reworked *Toweius pertusus* is similar to that of the other two autochthonous taxa. These characteristics indicate that dissolution was the main factor controlling carbonate content variations throughout the studied interval, although changes in calcification rates and even intervals with increased calcification cannot be ruled out.

The dissolution process most likely took place on the seabed. It was probably linked to a rise in the lysocline to approximately 1500 m, which resulted in the accumulation of carbonate barren sediments in North Atlantic abyssal sites. The available information suggests that the rise in the lysocline was the result of a shift in the location of deep water

sources. Bottom waters were generally formed in the Southern Ocean in Eocene times, but several previous studies have shown that downwelling weakened or even stopped in this area during hyperthermal events. Simultaneously, NW Atlantic downwelling began, which transported high pCO₂ corrosive waters downwards, causing a rise in the CCD and lysocline.

Acknowledgments

This research was funded by the Spanish Government project CGL2015-65404-R (MINECO/FEDER, EU), and by the Basque Government project IT-930-16. BI-Z received a pre-doctoral grant from the University of the Basque Country (UPV/EHU). Two anonymous reviewers provided comments which helped to improve the manuscript. Thanks are due to Carl Sheaver for his language corrections and to the Oceanic Geoscience Group (GGO) from Salamanca with special mention to Jose Ignacio Martin, for their help in calcareous nannofossil sample preparation and analysis.

References

- Adelseck Jr., C.G., Geehan, G.W., Roth, P.H., 1973. Experimental evidence for the selective dissolution and overgrowth of calcareous nannofossils during diagenesis. *Geol. Soc. Am. Bull.* 84, 2755–2762. [http://dx.doi.org/10.1130/0016-7606\(1973\)84<2755:EEFTSD>2.0.CO;2](http://dx.doi.org/10.1130/0016-7606(1973)84<2755:EEFTSD>2.0.CO;2).
- Agnini, C., Fornaciari, E., Rio, D., Tateo, F., Backman, J., Giusberti, L., 2007. Responses of calcareous nannofossil assemblages, mineralogy and geochemistry to the environmental perturbations across the Paleocene/Eocene boundary in the Venetian Pre-Alps. *Mar. Micropaleontol.* 63, 19–38. <http://dx.doi.org/10.1016/j.marmicro.2006.10.002>.
- Agnini, C., Macri, P., Backman, J., Brinkhuis, H., Fornaciari, E., Giusberti, L., Luciani, V., Rio, D., Sluijs, A., Speranza, F., 2009. An early Eocene carbon cycle perturbation at ~52.5 Ma in the Southern Alps: chronology and biotic response. *Paleoceanography* 24, 2209–2222. <http://dx.doi.org/10.1029/2008PA001649>.
- Agnini, C., Fornaciari, E., Raffi, I., Catanzariti, R., Pälike, H., Backman, J., Rio, D., 2014. Biozonation and biochronology of Paleogene calcareous nannofossils from low and middle latitudes. *Newsl. Stratigr.* 47 (2), 131–181. <http://dx.doi.org/10.1127/0078-0421/2014/0042>.
- Agnini, C., Spofforth, D.J.A., Dickens, G.R., Rio, D., Pälike, H., Backman, J., Muttoni, G., Dallanave, E., 2015. Stable isotope and calcareous nannofossil assemblage records for the Cicogna section: toward a detailed template of late Paleocene and early Eocene global carbon cycle and nanoplankton evolution. *Clim. Past Discuss.* 11, 4329–4389. <http://dx.doi.org/10.5194/cp-12-883-2016>.
- Agnini, C., de Bernardi, B., Erba, E., 2016. Volume and carbonate production estimates of early Palaeogene calcareous nannofossils. *Lethaia* 50 (1), 58–68. <http://dx.doi.org/10.1111/let.12176>.
- Alexander, K., Meissner, K.J., Bralower, T.J., 2015. Sudden spreading of corrosive bottom water during the Palaeocene-Eocene thermal maximum. *Nat. Geosci.* 8, 458–462. <http://dx.doi.org/10.1038/ngeo2430>.
- Archer, D., 1999. Modeling CO₂ in the ocean: A review. In: Bouwman, A.F. (Ed.), *Scaling of Trace Gas Fluxes between Terrestrial and Aquatic Ecosystems and the Atmosphere, Developments in Atmospheric Science*, 24. Elsevier Sciences, Amsterdam, pp. 169–184.
- Bains, S., Corfield, R.M., Norris, R.D., 1999. Mechanisms of climate warming at the end of the Paleocene. *Science* 285, 724–727. <http://dx.doi.org/10.1126/science.285.5428.724>.
- Baumann, K.H., Adrulite, H., Boeckel, B., Geisen, M., Kinkel, H., 2005. The significance of extant coccolithophores as indicators of ocean water masses, surface water temperature, and palaeoproductivity: a review. *Palaeontol. Z.* 79, 93–112. <http://dx.doi.org/10.1007/BF03021756>.
- Beaufort, L., Probert, I., de Garidel-Thoron, T., Bendif, E.M., Ruiz-Pino, D., Metzl, N., Goyet, C., Buchet, N., Coupel, P., Grelaud, M., Rost, B., Rickaby, R.E., de Vargas, C., 2011. Sensitivity of coccolithophores to carbonate chemistry and ocean acidification. *Nature* 476, 80–83. <http://dx.doi.org/10.1038/nature10295>.
- Beaufort, L., Barbarin, N., Gally, Y., 2014. Optical measurements to determine the thickness of calcite crystals and the mass of thin carbonate particles such as coccoliths. *Nat. Protoc.* 9, 633–642. <http://dx.doi.org/10.1038/nprot.2014.028>.
- Bernaola, G., Orue-Etxebarria, X., Payros, A., Dinarès-Turell, J., Tosquella, J., Apellaniz, E., Caballero, F., 2006. Biomagnetostratigraphic analysis of the Gorrondatxe section (Basque Country, Western Pyrenees): its significance for the definition of the Ypresian/Lutetian boundary stratotype. *Neues Jb. Geol. Paläontol. Abh.* 241, 67–109.
- Bice, K.L., Marotzke, J., 2000. Warm climate dynamics. *GFF* 122, 29–30. <http://dx.doi.org/10.1080/11035890001221029>.
- Bice, K.L., Marotzke, J., 2002. Could changing ocean circulation have destabilized methane hydrate at the Paleocene/Eocene boundary? *Paleoceanography* 17 (2), 8.1–8.12. <http://dx.doi.org/10.1029/2001PA000678>.
- Bolton, C.T., Stoll, H.M., 2013. Late Miocene threshold response of marine algae to carbon dioxide limitation. *Nature* 500, 558–562. <http://dx.doi.org/10.1038/nature12448>.
- Bornemann, A., Norris, R.D., Lyman, J.A., d'Haenens, S., Groeneveld, J., Röhle, U., Farley, K.A., Speijer, R.P., 2014. Persistent environmental change after the Paleocene-Eocene Thermal Maximum in the eastern North Atlantic. *Earth Planet. Sci. Lett.* 394, 70–81. <http://dx.doi.org/10.1016/j.epsl.2014.03.017>.
- Bown, P.R., 1998. *Calcareous Nannofossil Biostratigraphy*. British micropaleontological society publication series. Chapman & Hall, Kluwer Academic & Lipincott-Raven Publishers, London (ISBN 13: 978-9401060561).
- Bralower, T.J., 2002. Evidence of surface water oligotrophy during the Paleocene-Eocene Thermal Maximum: Nannofossil assemblage data from ocean drilling program Site 690, Maud Rise, Weddell Sea. *Paleoceanography* 17 (2), 1029–1042. <http://dx.doi.org/10.1029/2001PA000662>.
- Bralower, T.J., Self-Trial, J.M., 2016. Nannoplankton malformation during the Paleocene-Eocene Thermal Maximum and its paleoecological and paleoceanographic significance. *Paleoceanography* 31, 1423–1439. <http://dx.doi.org/10.1002/2016PA002980>.
- Bralower, T.J., Kelly, D.C., Gibbs, S.J., Farley, K., Eccles, L., Lindemann, T.L., Smith, G.J., 2014. Impact of dissolution on the sedimentary record of the Paleocene-Eocene thermal maximum. *Earth Planet. Sci. Lett.* 401, 70–82. <http://dx.doi.org/10.1016/j.epsl.2014.05.055>.
- Caldeira, K., Wickett, M.E., 2005. Ocean model predictions of chemistry changes from carbon dioxide emissions to the atmosphere and ocean. *J. Geophys. Res.* 110, C09S04. <http://dx.doi.org/10.1029/2004JC002671>.
- Colosimo, A.B., Bralower, T.J., Zachos, J.C., 2006. Evidence for lysocline shoaling at the Paleocene/Eocene Thermal Maximum on Shatsky Rise, Northwest Pacific. *Proc. Ocean Drill. Program Sci. Results* 198, 1–36. <http://dx.doi.org/10.2973/odp.proc.sr.198.112.2006>.
- Cope, J.T., Winguth, A.M.E., 2011. On the sensitivity of ocean circulation to arctic freshwater input during the Paleocene/Eocene thermal maximum. *Palaeogeogr. Palaeoclimatol. Palaeoecol.* 306 (1–2), 82–94. <http://dx.doi.org/10.1016/j.palaeo.2011.03.032>.
- Cramer, B.S., Wright, J.D., Kent, D.V., Aubrey, M.P., 2003. Orbital climate forcing of δ¹³C excursions in the late Paleocene - early Eocene (chrons C24n–C25n). *Paleoceanography* 18 (4), 1097–1117. <http://dx.doi.org/10.1029/2003PA000909>.
- Dedert, M., Stoll, H., Kars, S., Young, J.R., Shimizu, N., Kroon, D., Lourens, L., Ziveri, P., 2014. Temporally variable diagenetic overgrowth on deep-sea nannofossil carbonates across Palaeogene hyperthermals and implications for isotopic analyses. *Mar. Micropaleontol.* 107, 18–31. <http://dx.doi.org/10.1016/j.marmicro.2013.12.004>.
- Denman, K.L., Brasseur, G., Chidhaisong, A., Caias, P., Cox, P.M., Dickinson, R.E., Hauglustaine, D., Heinze, C., Holland, E., Jacob, D., Lohmann, U., Ramachandran, S., Dias, P.L.S., Wofsy, S.C., Zhang, X., 2007. Couplings between changes in the climate system and biogeochemistry. In: Solomon, S., Qin, D., Manning, M., Chen, Z., Marquis, M., Averyt, K.B., Tignor, M., Miller, H.L. (Eds.), *Climate Change 2007: The Physical Science Basis. Contribution of Working Group I to the Fourth Assessment Report of the Intergovernmental Panel on Climate Change*. Cambridge University Press, Cambridge and New York, pp. 499–587.
- Dickens, G.R., 2003. Rethinking the global carbon cycle with a large dynamic and microbially mediated gas hydrate capacitor. *Earth Planet. Sci. Lett.* 213, 169–183. [http://dx.doi.org/10.1016/S0012-821X\(03\)00325-X](http://dx.doi.org/10.1016/S0012-821X(03)00325-X).
- Dickens, G.R., Castillo, M.M., Walker, J.C.G., 1997. A blast of gas in the latest Paleocene: simulating first-order effects of massive dissociation of oceanic methane hydrate. *Geology* 25, 259–262. [http://dx.doi.org/10.1130/0091-7613\(1997\)025<259:ABOGIT>2.3.CO;2](http://dx.doi.org/10.1130/0091-7613(1997)025<259:ABOGIT>2.3.CO;2).
- Dunkley Jones, T., Lunt, D.J., Schmidt, D.N., Ridgwell, A., Sluijs, A., Valdes, P.J., Maslin, M., 2013. Climate model and proxy data constraints on ocean warming across the Paleocene-Eocene Thermal Maximum. *Earth-Sci. Rev.* 125, 123–145. <http://dx.doi.org/10.1016/j.earscirev.2013.07.004>.
- Firth, J.V., Eldrett, J.S., Harding, I.C., Coxall, H.K., Wade, B.S., 2012. Palaeoceanographic Events from High to Low Latitudes of ODP Hole 647A: Implications for Correlating Integrated Biomagnetochronology for the Palaeogene. *373 Geological Society, London (Special Publications)*.
- Flores, J.A., Siervo, F.J., 1997. Revised technique for calculation of calcareous nannofossil accumulation rates. *Micropaleontology* 43, 321–324. <http://dx.doi.org/10.2307/1485832>.
- Forster, P., Ramaswamy, V., Artaxo, P., Berntsen, T., Betts, R., Fahey, D.W., Haywood, J., Lean, J., Lowe, D.C., Myhre, G., Nganga, J., Prinn, R., Raga, G., Schulz, M., Van Dorland, R., 2007. Changes in atmospheric constituents and in radiative forcing. In: Solomon, S., Qin, D., Manning, M., Chen, Z., Marquis, M., Averyt, K.B., Tignor, M., Miller, H.L. (Eds.), *Climate Change 2007: The Physical Basis. Contribution of Working Group I to the Fourth Assessment Report of the Intergovernmental Panel on Climate Change*. Cambridge University Press, Cambridge, pp. 131–234.
- Fuentes, M.A., Flores, J.A., Siervo, F.J., 2014. The use of circularly polarized light for biometry, identification and estimation of mass of coccoliths. *Mar. Micropaleontol.* 113, 44–55. <http://dx.doi.org/10.1016/j.marmicro.2014.08.007>.
- Galeotti, S., Krishnan, S., Pagani, M., Lanzi, L., Gaudio, A., Zachos, J.C., Monechi, S., Morelli, G., Lourens, L., 2010. Orbital chronology of early Eocene hyperthermals from the Contessa Road section, central Italy. *Earth Planet. Sci. Lett.* 290, 192–200. <http://dx.doi.org/10.1016/j.epsl.2009.12.021>.
- Gibbs, S.J., Shackleton, N.J., Young, J.R., 2004. Identification of dissolution patterns in nannofossil assemblages: a high-resolution comparison of synchronous records from Ceará Rise, ODP Leg 154. *Paleoceanography* 19, PA1029. <http://dx.doi.org/10.1029/2003.marmicro.2003.09.002>.
- Gibbs, S.J., Bralower, T.J., Bown, P.R., Zachos, J.C., Bybell, L.M., 2006. Shelf and open-ocean calcareous phytoplankton assemblages across the Paleocene–Eocene thermal maximum: implications for global productivity gradients. *Geology* 34 (4), 233–236. <http://dx.doi.org/10.1130/G22381.1>.
- Gibbs, S.J., Stoll, H.M., Bown, P.R., Bralower, T.J., 2010. Ocean acidification and surface

- water carbonate production across the Paleocene–Eocene thermal maximum. *Earth Planet. Sci. Lett.* 295, 583–592. <http://dx.doi.org/10.1016/j.epsl.2010.04.044>.
- Giusberti, L., Rio, D., Agnini, C., Backman, J., Fornaciari, E., Tateo, F., Oddone, M., 2007. Mode and tempo of the Paleocene–Eocene Thermal Maximum in an expanded section from the Venetian pre-Alps. *Geol. Soc. Am. Bull.* 119 (3–4), 391–412. <http://dx.doi.org/10.1130/B25994.1>.
- Gradstein, F.M., Ogg, J.G., Schmitz, M., Ogg, G., 2012. *The Geologic Time Scale 2012*, 1st Edition. Elsevier, Amsterdam978-0444594488.
- d'Haenens, S., Bornemann, A., Claeys, P., Röhl, U., Steurbaut, E., Speijer, R.P., 2014. A transient deep-sea circulation switch during Eocene Thermal Maximum 2. *Paleoceanography* 29, 2567–2585. <http://dx.doi.org/10.1002/2013PA002567>.
- Hassenkam, T., Johnson, A., Bechgaard, K., Stipp, S.L., 2011. Tracking single coccolith dissolution with pictogram resolution and implications for CO₂ sequestration and ocean acidification. *Proc. Natl. Acad. Sci.* 108 (21), 8571–8576. <http://dx.doi.org/10.1073/pnas.1009447108>.
- Hobbein, M.W., Sexton, P.F., Cartwright, J.A., 2012. Onset of North Atlantic Deep Water production coincident with inception of the Cenozoic global cooling trend. *Geology* 40 (3), 255–258. <http://dx.doi.org/10.1130/G32461.1>.
- Hönisch, B., Ridgwell, A., Schmidt, D.N., Thomas, E., Gibbs, S.J., Sluijs, A., Zeebe, R., Kump, L., Martindale, R.C., Greene, S.E., Kiessling, W., Ries, J., Zachos, J.C., Royer, D.L., Barker, S., Marchitto, T.M., Moyer, R., Pelejero, C., Ziveri, P., Foster, G.L., Williams, B., 2012. The geological record of ocean acidification. *Science* 335, 1058–1063. <http://dx.doi.org/10.1126/science.1208277>.
- Iglesias-Rodríguez, M.D., Halloran, P.R., Rickaby, R.E.M., Hall, I.R., Colmenero-Hidalgo, E., Gittins, J.R., Green, D.R.H., Tyrrell, T., Gibbs, S.J., Von Dassow, P., Rehm, E., Armburst, E.V., Boessenkool, K.P., 2008. Phytoplankton calcification in a high-CO₂ world. *Science* 320, 336–340. <http://dx.doi.org/10.1126/science.1154122>.
- Intxauspe-Zubiaurre, B., Payros, A., Flores, J.A., Apellaniz, E., 2017. Changes to sea-surface characteristics during the middle Eocene (47.4 Ma) C21r-H6 event: evidence from calcareous nannofossil assemblages of the Gorrondate section (western Pyrenees). *Newsl. Stratigr.* 50 (3), 245–267. <http://dx.doi.org/10.1127/nos/2017/0305>.
- Jennions, S.M., Thomas, E., Schmidt, D.N., Lunt, D., Ridgwell, A., 2015. Changes in benthic ecosystems and ocean circulation in the Southeast Atlantic across Eocene Thermal Maximum 2. *Paleoceanography* 30, 1059–1077. <http://dx.doi.org/10.1002/2015PA002821>.
- Jiang, S., Wise, S.W., 2006. Surface water chemistry and fertility variations in the tropical Atlantic across the Paleocene/Eocene Thermal Maximum as evidenced by calcareous nannoplankton from ODP Leg 207, Hole 1259B. *Rev. Micropaleontol.* 49, 227–244. <http://dx.doi.org/10.1016/j.revmic.2006.10.002>.
- Keeling, C.D., Whorf, T.P., 2004. Atmospheric carbon dioxide record from Mauna Loa, in Oak Ridge Laboratory Trends: a compendium of data on global change. In: Carbon Dioxide Information Analysis Center, Oak Ridge National Laboratory. U.S.A. Department of Energy, Oak Ridge, Tennessee, U.S.A. <http://dx.doi.org/10.3334/CDIAC/atg.035>.
- Kelly, D.C., Zachos, J.C., Bralower, T.J., Schellenberg, S.A., 2005. Enhanced terrestrial weathering/runoff and surface ocean carbonate production during the recovery stages of the Paleocene–Eocene thermal maximum. *Paleoceanography* 20, PA4023. <http://dx.doi.org/10.1029/2005PA001163>.
- Kelly, D.C., Nielsen, T.M.J., Schellenberg, S.A., 2012. Carbonate saturation dynamics during the Paleocene–Eocene thermal maximum: bathyal constraints from ODP Sites 689 and 690 in the Weddell Sea (South Atlantic). *Mar. Geol.* 103–106, 75–86. <http://dx.doi.org/10.1016/j.margeo.2012.02.003>.
- Kennett, J.P., Stott, L.D., 1991. Abrupt deep-sea warming, paleoceanographic changes and benthic extinctions. *Nature* 353, 225–229. <http://dx.doi.org/10.1038/353225a0>.
- Khalil, H., Al Sawy, S., 2014. Integrated biostratigraphy, stage boundaries and Paleoclimatology of the Upper Cretaceous–Lower Eocene successions in Kharga and Dakhla Oases, Western Desert, Egypt. *J. Afr. Earth Sci.* 96, 220–242. <http://dx.doi.org/10.1016/j.jafrearsci.2014.04.010>.
- Kirtland Turner, S., Sexton, P.F., Charles, C.D., Norris, R.D., 2014. Persistence of carbon release events through the peak of early Eocene global warmth. *Nat. Geosci.* 7, 748–751. <http://dx.doi.org/10.1038/ngeo2240>.
- Kump, L.R., Bralower, T.J., Ridgwell, A., 2009. Ocean acidification in deep time. *Oceanography* 20 (22), 94–107. <http://dx.doi.org/10.5670/oceanog.2009.100>.
- Langer, G., Geisen, M., Baumann, K.H., Klas, J., Riebesell, U., Thoms, S., Young, J.R., 2006. Species-specific responses of calcifying algae to changing seawater carbonate chemistry. *Geochem. Geophys. Geosyst.* 7, 1227–1238. <http://dx.doi.org/10.1029/2005GC001227>.
- Lei, Y., Jiang, S., Wise, S.W., Cui, Y., Wang, Y., 2016. Contrasting response of the calcareous nannoplankton communities after the Eocene hyperthermal events in the tropical Atlantic Ocean. *Mar. Micropaleontol.* 129, 24–31. <http://dx.doi.org/10.1016/j.marmicro.2016.11.001>.
- Leon-Rodríguez, L., Dickens, G.R., 2010. Constraints on ocean acidification associated with rapid and massive carbon injections: the early Paleogene record at Ocean Drilling Program Site 1215, Equatorial Pacific Ocean. *Palaeogeogr. Palaeoclimatol. Palaeoecol.* 298, 409–420. <http://dx.doi.org/10.1016/j.palaeo.2010.10.029>.
- Lourens, J.L., Sluijs, A., Kroon, D., Zachos, J.C., Thomas, E., Röhl, U., Bowles, J., Raffi, I., 2005. Astronomical pacing of late Paleocene to early Eocene global warming events. *Nature* 435, 1083–1087. <http://dx.doi.org/10.1038/nature03814>.
- Lunt, D.J., Valdes, P.J., Jones, T.D., Ridgwell, A., Haywood, A., Schmidt, D.N., Marsh, R., Maslin, M., 2010. CO₂-driven ocean circulation changes as an amplifier of Paleocene–Eocene Thermal Maximum hydrate destabilization. *Geology* 38 (10), 875–878. <http://dx.doi.org/10.1130/G31184.1>.
- Lunt, D.J., Dunkley Jones, T., Heinemann, M., Huber, M., LeGrande, A., Winguth, A., Lopston, C., Marotzke, J., Roberts, C.D., Tindall, J., Valdes, P., Winguth, C., 2012. A model-data comparison for a multi-model ensemble of early Eocene atmosphere–ocean simulations: EoMIP. *Clim. Past* 8 (5), 1717–1736. <http://dx.doi.org/10.5194/cp-8-1717-2012>.
- Maier-Reimer, E., Hasselmann, K., 1987. Transport and storage of CO₂ in the ocean – an inorganic ocean-circulation carbon cycle model. *Clim. Dyn.* 2, 63–90. <http://dx.doi.org/10.1007/BF01054491>.
- Martini, E., 1971. Standard Tertiary and Quaternary calcareous nanoplankton zonation. In: Farinacci, A. (Ed.), *Proceedings of the Second International Conference on Planktonic Microfossils Roma, Rome*. 2. Ed. Tecnosc., pp. 739–785.
- Meyer, J., Riebesell, U., 2015. Reviews and syntheses: responses of coccolithophores to ocean acidification: a meta-analysis. *Biogeosciences* 12, 1671–1682. <http://dx.doi.org/10.5194/bg-12-1671-2015>.
- Milliman, J.D., 1999. Production and accumulation of calcium carbonate in the ocean: budget of a nonsteady state. *Glob. Biogeochem. Cycles* 7, 927–957. <http://dx.doi.org/10.1029/93GB02524>.
- Molina, E., Alegret, L., Apellaniz, E., Bernaola, G., Caballero, F., Dinarès-Turell, J., Hardenbol, J., Heilmann-Clausen, C., Larrasoña, J.C., Luterbacher, H., Monecchia, S., Ortiz, S., Orue-Etxebarria, X., Payros, A., Pujalte, V., Rodríguez-Tovar, F.J., Toris, F., Tosquella, J., Uchman, A., 2011. The Global Stratotype Section and Point (GSSP) for the base of the Lutetian Stage at the Gorrondate section, Spain. *Episodes* 34 (2), 86–108.
- Montadert, L., Roberts, D.G., 1979. Initial reports of the Deep Sea Drilling Project. 48 Government Printing Office, Washington. <http://dx.doi.org/10.2973/dspd.proc.48.1979>.
- Monteiro, F.M., Bach, L.T., Brownlee, C., Bown, P., Rickaby, R.E.M., Pulton, A.J., Tyrrell, T., Beaufort, L., Dutkiewicz, S., Gibbs, S., Gutowska, M.A., Lee, R., Riebesell, U., Young, J., Ridgwell, A., 2016. Why marine phytoplankton calcify. *Sci. Adv.* 2 (7). <http://dx.doi.org/10.1126/sciadv.1501822>.
- Mutterlose, J., Linnert, C., Norris, R., 2007. Calcareous nannofossils from the Paleocene–Eocene Thermal Maximum of the equatorial Atlantic (ODP Site 1260B): evidence for tropical warming. *Mar. Micropaleontol.* 65, 13–31. <http://dx.doi.org/10.1016/j.marmicro.2007.05.004>.
- Nicol, M.J., Dickens, G.R., Hollis, C.J., Zachos, J.C., 2007. Multiple early Eocene hyperthermals: their sedimentary expression on the New Zealand continental margin and in the deep sea. *Geology* 35 (8), 699–702. <http://dx.doi.org/10.1130/G23648A.1>.
- Norris, R.D., Wilson, P.A., Blum, P., Expedition 342 Scientists, 2012. Paleogene Newfoundland sediment drifts. *IODP Prelim. Rep.* 342, 1–263. <http://dx.doi.org/10.2204/iodp.pr.342.2012>.
- Nunes, F., Norris, R.D., 2006. Abrupt reversal in ocean overturning during the Palaeocene/Eocene warm period. *Nature* 439, 60–63. <http://dx.doi.org/10.1038/nature04386>.
- O'Dea, S.A., Gibbs, S.J., Bown, P.R., Young, J.R., Poulton, A.J., Newsam, C., Wilson, P.A., 2014. Coccolithophore calcification response to past ocean acidification and climate change. *Nat. Commun.* 5, 5363. <http://dx.doi.org/10.1038/ncomms6363>.
- Okada, H., Bukry, D., 1980. Supplementary modification and introduction of code numbers of the low-latitude coccolith biostratigraphic zonation (Bukry, 1973; 1975). *Mar. Micropaleontol.* 5, 321–325.
- Orr, J.C., Fabry, V.J., Autumont, O., Bopp, L., Doney, S.C., Feely, R.A., Gnanadesikan, A., Gruber, N., Ishida, A., Joos, F., et al., 2005. Anthropogenic ocean acidification over the twenty-first century and its impact on calcifying organisms. *Nature* 437, 681–686. <http://dx.doi.org/10.1038/nature04095>.
- Pak, D.K., Miller, K.G., 1992. Paleocene to Eocene benthic foraminiferal isotopes and assemblages: Implications for deepwater circulation. *Paleoceanography* 7 (4), 405–422. <http://dx.doi.org/10.1029/92PA01234>.
- Páliike, H., Lyle, M.W., Nishi, H., Raffi, I., Ridgwell, A., Gamage, K., Klaus, A., Acton, G.D., Anderson, L., Backman, J., Baldauf, J.G., Beltran, C., Bohaty, S.M., Bown, P.R., Busch, W.H., Channell, J.E.T., Chun, C.O.J., Delaney, M.L., Dewang, P., Dunkley Jones, T., Edgar, K.M., Evans, H.F., Fitch, P., Foster, G.L., Gussone, N., Hasegawa, H., Hathorne, E.C., Hayashi, H., Herrle, J.O., Holbourn, A., Hovan, S.A., Hyeong, K., Iijima, K., Ito, T., Kamikuri, S.I., Kimoto, K., Kuroda, J., Leon-Rodríguez, L., Malinverno, A., Moore, T.C., Murphy, B., Murphy, D.P., Nakamura, H., Ogane, K., Ohneiser, C., Richter, C., Robinson, R.S., Rohling, E.J., Romero, O.E., Sawada, K., Scher, H.D., Schneider, L., Sluijs, A., Takata, H., Tian, J., Tsujimoto, A., Wade, B.S., Westerhold, T., Wilkens, R.H., Williams, T., Wilson, P.A., Yamamoto, Y., Yamamoto, S., Yamazaki, T., Zeebe, R.E., 2012. A Cenozoic record of the equatorial Pacific carbonate compensation depth. *Nature* 488, 609–614. <http://dx.doi.org/10.1038/nature11360>.
- Payros, A., Martínez-Bráceras, N., 2014. Orbital forcing in turbidite accumulation during the Eocene greenhouse interval. *Sedimentology* 61, 1411–1432. <http://dx.doi.org/10.1111/sed.12113>.
- Payros, A., Orue-Etxebarria, X., Pujalte, V., 2006. Covarying sedimentary and biotic fluctuations in Lower-Middle Eocene Pyrenean deep-sea deposits: Palaeoenvironmental implications. *Palaeogeogr. Palaeoclimatol. Palaeoecol.* 234, 258–276. <http://dx.doi.org/10.1016/j.palaeo.2005.10.013>.
- Payros, A., Bernaola, G., Orue-Etxebarria, X., Dinarès-Turell, J., Tosquella, J., Apellaniz, E., 2007. Reassessment of the Early–Middle Eocene biomagnetochronology based on evidence from the Gorrondate section (Basque Country, western Pyrenees). *Lethaia* 40, 183–195. <http://dx.doi.org/10.1111/j.1502-3931.2007.00016.x>.
- Payros, A., Orue-Etxebarria, X., Bernaola, G., Apellaniz, E., Dinarès-Turell, J., Tosquella, J., Caballero, F., 2009. Characterization and astronomically calibrated age of the first occurrence of *Turborotalita frontosa* in the Gorrondate section, a prospective Lutetian GSSP: implications for the Eocene time scale. *Lethaia* 42, 255–264. <http://dx.doi.org/10.1111/j.1502-3931.2008.00142.x>.
- Payros, A., Ortiz, S., Alegret, L., Orue-Etxebarria, X., Apellaniz, E., Molina, E., 2012. An early Lutetian carbon-cycle perturbation: insights from the Gorrondate section (western Pyrenees, Bay of Biscay). *Paleoceanography* 27, 2213–2226. <http://dx.doi.org/10.1029/2011PA01142>.

- [org/10.1029/2012PA002300](http://dx.doi.org/10.1029/2012PA002300).
- Payros, A., Ortiz, S., Millán, I., Arostegi, J., Orue-Etxebarria, X., Apellaniz, E., 2015. The Early Eocene Climatic Optimum: environmental impact on the North Iberian continental margin. *GSA Bull.* 127 (11–12), 1632–1644. <http://dx.doi.org/10.1130/B31278.1>.
- Penman, D.E., Höönsch, B., Zeebe, R.E., Thomas, E., Zachos, J.C., 2014. Rapid and sustained surface ocean acidification during the Paleocene–Eocene Thermal Maximum. *Paleoceanography* 29, 357–369. <http://dx.doi.org/10.1002/2014PA002621>.
- Perch-Nielsen, K., 1985. Cenozoic calcareous nannofossils. In: Bolli, H.M., Saunders, J.B., Perch-Nielsen, K. (Eds.), *Plankton Stratigraphy*. Cambridge University Press, Cambridge, pp. 427–554.
- Pujalte, V., Robador, A., Payros, A., Samsó, J.M., 2016. A siliciclastic braid delta within a lower Paleogene carbonate platform (Ordesa-Monte Perdido National Park, southern Pyrenees, Spain): Record of the Paleocene–Eocene Thermal Maximum perturbation. *Palaeogeogr. Palaeoclimatol. Palaeoecol.* 459, 453–470. <http://dx.doi.org/10.1016/j.palaeo.2016.07.029>.
- Raffi, I., de Bernardi, B., 2008. Response of calcareous nannofossils to the Paleocene–Eocene Thermal Maximum: observations on composition, preservation and calcification in sediments from ODP Site 1263 (Walvis Ridge – SW Atlantic). *Mar. Micropaleontol.* 69, 119–138. <http://dx.doi.org/10.1016/j.marmicro.2008.07.002>.
- Raffi, I., Backman, J., Pälike, H., 2005. Changes in calcareous nannofossil assemblages across the Paleocene/Eocene transition from the paleo-equatorial Pacific Ocean. *Palaeogeogr. Palaeoclimatol. Palaeoecol.* 226, 93–126. <http://dx.doi.org/10.1016/j.palaeo.2005.05.006>.
- Raffi, I., Backman, J., Zachos, J.C., Sluijs, A., 2009. The response of calcareous nannofossil assemblages to the Paleocene Eocene Thermal Maximum at the Walvis Ridge in the South Atlantic. *Mar. Micropaleontol.* 70, 201–212. <http://dx.doi.org/10.1016/j.marmicro.2008.12.005>.
- Raven, J.A., Crawford, K., 2012. Environmental controls on coccolithophore calcification. *Mar. Ecol. Prog. Ser.* 470, 137–166. <http://dx.doi.org/10.3354/meps09993>.
- Ravizza, G., Norris, R.N., Blusztajn, J., Aubrey, M.P., 2001. An osmium isotope excursion associated with the late Paleocene thermal maximum: evidence of intensified chemical weathering. *Paleoceanography* 16, 155–163. <http://dx.doi.org/10.1029/2000PA000541>.
- Rea, D.K., Lyle, M.W., 2005. Paleogene calcite compensation depth in the eastern subtropical Pacific: answers and questions. *Paleoceanography* 20, PA1012. <http://dx.doi.org/10.1029/2004PA001064>.
- Ridgwell, A., 2007. Interpreting transient carbonate compensation depth changes by marine sediment core modelling. *Paleoceanography* 22, PA4102. <http://dx.doi.org/10.1029/2006PA001372>.
- Ridgwell, A., Schmidt, D.N., 2010. Past constraints on the vulnerability of marine calcifiers to massive carbon dioxide release. *Nat. Geosci.* 3, 196–200. <http://dx.doi.org/10.1038/ngeo755>.
- Riebesell, U., 2004. Effects of CO₂ enrichment on marine phytoplankton. *J. Oceanogr.* 60, 719–729. <http://dx.doi.org/10.1007/s10872-004-5764-z>.
- Riebesell, U., Zondervan, I., Rost, B., Tortell, P.D., Zeebe, R.E., Morel, F.M.M., 2000. Reduced calcification of marine plankton in response to increased atmospheric CO₂. *Nature* 407, 364–367.
- Rivero-Calle, S., Gnanadesikan, A., del Castillo, C.E., Balch, W.M., Guikema, S.D., 2015. Multidecadal increase in North Atlantic coccolithophores and the potential role of rising CO₂. *Science* 350, 1533–1537. <http://dx.doi.org/10.1126/science.aaa8026>.
- Roberts, C.D., Le Grande, A.N., Tripati, A.K., 2009. Climate sensitivity to arctic seaway restriction during the Early Paleogene. *Earth Planet. Sci. Lett.* 286, 576–585. <http://dx.doi.org/10.1016/j.epsl.2009.07.026>.
- Röhl, U., Westerhold, T., Monechi, S., Thomas, E., Zachos, J.C., Donner, B., 2005. The Third and Final Early Eocene Thermal Maximum: Characteristics, Timing and Mechanisms of the 'X' Event, GSA Annual Meeting 37. Geological Society of America, Salt Lake City (SRef-ID: 1607-7962/gru/EGU06-A-04560).
- Rost, B., Riebesell, U., 2004. Coccolithophores and the biological pump: responses to environmental changes. In: Thierstein, H.R., Young, J.R. (Eds.), *Coccolithophores – From Molecular Processes to Global Impact*. Springer, Berlin, pp. 99–125. <http://dx.doi.org/10.1013/epic.21851.d001>.
- Rudimann, W.F., 2001. Orbital-scale changes in carbon dioxide and methane. In: Rudimann, W.F. (Ed.), *Earth's Climate. Past and future*. W.F. Freeman and Company, pp. 234–253.
- Sarmiento, J.L., Siegenthaler, U., Orr, J.C., 1992. A perturbation simulation of CO₂ uptake in an ocean general circulation model. *J. Geophys. Res.* 97, 3621–3645. <http://dx.doi.org/10.1029/91JC02849>.
- Schaller, M.F., 2015. Paleoceanography: corrosive circulation. *Nat. Geosci.* 8, 429–430. <http://dx.doi.org/10.1038/ngeo2446>.
- Schmitz, B., Pujalte, V., 2003. Sea-level, humidity, and land-erosion records across the initial Eocene Thermal Maximum from a continental-marine transect in northern Spain. *Geology* 31 (8), 689–692. <http://dx.doi.org/10.1130/G19527.1>.
- Sexton, P.F., Norris, R.D., Wilson, P.A., Pälike, H., Westerhold, T., Röhl, U., Bolton, C.T., Gibbs, S.J., 2011. Eocene global warming events driven by ventilation of oceanic dissolved organic carbon. *Nature* 471, 349–352. <http://dx.doi.org/10.1038/nature09826>.
- Sluijs, A., Bowen, G., Brinkhuis, H., Lourens, L., Thomas, E., 2007a. The Palaeocene–Eocene Thermal Maximum Super Greenhouse: Biotic and Geochemical Signatures. Age Models and Mechanisms of Global Change, Deep-Time Perspectives on Climate Change: Marrying the Signal from Computer Models and Biological Proxies. 323–349. The Micropaleontological Society (Special Publications).
- Sluijs, A., Brinkhuis, H., Schouten, S., Bohaty, S.M., John, C.M., Zachos, J.C., Reichart, G.J., Sissinghe Damsté, J.S., Crouch, E.M., Dickens, G.R., 2007b. Environmental precursors to rapid light carbon injection at the Palaeocene/Eocene boundary. *Nature* 450, 1218–1221. <http://dx.doi.org/10.1038/nature06400>.
- Sluijs, A., Schouten, S., Donders, T.H., Schoon, P.L., Röhl, U., Reichart, G.J., Sangiorgi, F., Kim, J.H., Sissinghe Damsté, J.S., Brinkhuis, H., 2009. Warm and wet conditions in the Arctic region during Eocene Thermal Maximum 2. *Nat. Geosci.* 2, 777–780. <http://dx.doi.org/10.1038/ngeo668>.
- Smith, A.G., 1996. Cenozoic latitudes, positions and topography of the Iberian Peninsula. In: Friend, P.F., Dabrio, C.J. (Eds.), *Tertiary basins of Spain: the stratigraphic record of crustal kinematics*. Cambridge University Press, Cambridge, pp. 6–8. <http://dx.doi.org/10.1017/CBO9780511524851.005>.
- Srivastava, S.P., Arthur, M., Clement, B., Aksu, A., Baldauf, J., Bohrmann, G., Busch, W., Cederberg, T., Cremer, M., Daday, K., De Vernal, A., Firth, J., Hall, F., Head, M., Hiscott, R., Jarrard, R., Kaminski, M., Lazarus, D., Monjanel, A.L., Nielsen, O.B., Stein, R., Thiebaud, F., Zachos, J., Zimmermann, H., 1987. Proceedings of the Ocean Drilling Program, Scientific Results. 105 College Station, Texas (Ocean Drilling Program). <http://dx.doi.org/10.2973/odp.proc.ir.105.1987>.
- Stap, L., Sluijs, A., Thomas, E., Lourens, L., 2009. Patterns and magnitude of deep sea carbonate dissolution during Eocene Thermal Maximum 2 and H₂, Walvis Ridge, South-Eastern Atlantic Ocean. *Paleoceanography* 24, 1211–1223. <http://dx.doi.org/10.1029/2008PA001655>.
- Stoll, H.M., Shimizu, N., Archer, D., Ziveri, P., 2007. Coccolithophore productivity response to greenhouse event of the Paleocene–Eocene Thermal Maximum. *Earth Planet. Sci. Lett.* 258, 192–206. <http://dx.doi.org/10.1016/j.epsl.2007.03.037>.
- Thierstein, H.R., Young, J.R., 2004. *Coccolithophores: From Molecular Processes to Global Impact*. Springer, Berlin Heidelberg.
- Thomas, E., Shackleton, N.J., 1996. The Paleocene–Eocene benthic foraminiferal extinction and stable isotope anomalies. In: Knox, R.W.O.B., Corfield, R.M., Dunay, R.E. (Eds.), *Correlation of the Early Paleogene in Northwest Europe*. 101. Geological Society Special Publication, pp. 401–441. <http://dx.doi.org/10.1144/GSL.SP.1996.101.01.20>.
- Thomas, E., Zachos, J.C., 2000. Was the late Paleocene Thermal Maximum a unique event? *GFF* 122 (1), 169–170. <http://dx.doi.org/10.1080/11035890001221169>.
- Thomas, D.J., Bralower, T.J., Jones, C.E., 2003. Neodymium isotopic reconstruction of late Paleocene–early Eocene thermohaline circulation. *Earth Planet. Sci. Lett.* 209 (3–4), 309–322. [http://dx.doi.org/10.1016/S0012-821X\(03\)00096-7](http://dx.doi.org/10.1016/S0012-821X(03)00096-7).
- Tremolada, F., Bralower, T.J., 2004. Nannofossil assemblage fluctuations during the Paleocene–Eocene Thermal Maximum at Sites 213 (Indian Ocean) and 401 (North Atlantic Ocean): paleoceanographic implications. *Mar. Micropaleontol.* 52, 107–116. <http://dx.doi.org/10.1016/j.marmicro.2004.04.002>.
- Tripathi, A.K., Elderfield, H., 2005. Deep-sea temperature and circulation changes at the Paleocene–Eocene thermal maximum. *Science* 308, 1894–1898. <http://dx.doi.org/10.1126/science.1109202>.
- Weiss, R., 1974. Carbon dioxide in water and seawater. The solubility of a non-ideal gas. *Mar. Chem.* 2, 203–215. [http://dx.doi.org/10.1016/0304-4203\(74\)90015-2](http://dx.doi.org/10.1016/0304-4203(74)90015-2).
- Westbroek, P., Byrdemeier, B., Coleman, M., Dok, D.J., Fautin, D., Stal, L., Doumenge, F., 1994. Strategies for the study of climate forcing by calcification. In: *Past and Present Biomineralization Processes. Considerations About the Carbonate Cycle*. 13. Bulletin de l'Institut océanographique, Monaco, pp. 37–60.
- Westerhold, T., Röhl, U., Laskar, J., Raffi, I., Bowles, J., Lourens, L.J., Zachos, J.C., 2007. On the duration of magnetochrons C24r and C25n and the timing of early Eocene global warming events: implications from the Ocean Drilling Program Leg 208 Walvis Ridge depth transect. *Paleoceanography* 22, PA2201. <http://dx.doi.org/10.1029/2006PA001322>.
- Zachos, J.C., Pagani, M., Sloan, L., Thomas, E., Billups, K., 2001. Trends, rhythms and aberrations in global climate 65 Ma to present. *Science* 292, 686–693. <http://dx.doi.org/10.1126/science.1059412>.
- Zachos, J.C., Röhl, U., Schellenberg, S.A., Sluijs, A., Hodell, D.A., Kelly, D.C., Thomas, E., Niclou, M., Raffi, I., Lourens, L.J., McCarren, H., Kroon, D., 2005. Rapid acidification of the ocean during the Paleocene–Eocene Thermal Maximum. *Science* 308, 1611–1615. <http://dx.doi.org/10.1126/science.1109004>.
- Zachos, J.C., Dickens, G.R., Zeebe, R.E., 2008. An early Cenozoic perspective on greenhouse warming and carbon-cycle dynamics. *Nature* 451, 279–293. <http://dx.doi.org/10.1038/nature06588>.
- Zachos, J.C., McCarren, H., Murphy, B., Röhl, U., Westerhold, T., 2010. Tempo and scale of late Paleocene and early Eocene carbon isotope cycles: implications for the origin of hyperthermals. *Earth Planet. Sci. Lett.* 299, 242–249. <http://dx.doi.org/10.1016/j.epsl.2010.09.004>.
- Zeebe, R.E., 2013. What caused the long duration of the Paleocene–Eocene Thermal Maximum? *Paleoceanography* 28, 440–452. <http://dx.doi.org/10.1002/palo.20039>.
- Zeebe, R.E., Zachos, J.C., 2007. Reversed deep-sea carbonate ion basin gradient during Paleocene–Eocene thermal maximum. *Paleoceanography* 22. <http://dx.doi.org/10.1029/2006PA001395>.
- Zeebe, R.E., Zachos, J.C., Dickens, G.R., 2009. Carbon dioxide forcing alone insufficient to explain Paleocene–Eocene Thermal Maximum warming. *Nat. Geosci.* 2, 576–580. <http://dx.doi.org/10.1038/ngeo578>.
- Ziveri, P., Young, J.R., van Hinte, J.E., 1999. Coccolithophore export production and accumulation rates. In: Bruns, P., Hass, H.C. (Eds.), *On Determination of Sediment Accumulation Rates, GeoResearch Forum*. 5. Trans Tech Publications LTD, Switzerland, pp. 41–56.